This paper has to be cited as: ***Dai, K., Li, Z., Xu, Q., Tomas, R., Li, T., Jiang, L., Zhang, J., Yin, T. & Wang, H. 2023. Identification and evaluation of the high mountain upper slope potential landslide based on multi-source remote sensing: the Aniangzhai landslide case study. Landslides, doi: 10.1007/s10346-023-02044-4.*** The final publication is available at Springer via: https://link.springer.com/article/10.1007/s10346-023-02044-4

Identification and evaluation of the high mountain upper-slope potential landslide based on multi-source remote sensing: the Aniangzhai landslide case study

Keren Dai[1,2], Zhiyu Li[2], Qiang Xu[1*], Roberto Tomás[3], Tao Li[4], Liming Jiang[5], Jianyong Zhang[2], Tao Yin[2], Hao Wang[2]

[1] State Key Laboratory of Geohazard Prevention and Geoenvironment Protection, Chengdu University of Technology, Chengdu, China;

[2] College of Earth Sciences, Chengdu University of Technology, Chengdu, China;

[3] Departamento de Ingeniería Civil, Escuela Politécnica Superior, Universidad de Alicante, P.O. Box 99, E-03080 Alicante, Spain;

[4] Global Navigation Satellite System Research Center, Wuhan University, Wuhan 430079, China;

[5] Chengdu Jiujiang Weiye Technology Co., Ltd, Chengdu 610083, China;

* Correspondence: xq@cdut.edu.cn

Abstract: On June 17, 2020, Aniangzhai landslide, an ancient landslide located in Danba County, southwest China, was reactivated by Meilonggou debris flow. The front edge of the slope collapsed, mobilizing a soil mass of about 2.35×10^6 m^3. Evaluating the stability of the whole slope is of great importance to avoid further landslides and mitigate the damage for Aniangzhai villagers living on this slope. This paper focuses on the inaccessible upper-slope of Aniangzhai landslide (no attention paid before) that exhibits a relative elevation difference of more than 1000 m. Multi-source remote sensing including Unmanned Aerial Vehicle (UAV) photogrammetry, Light Detection and Ranging (LiDAR), and satellite-based Interferometric Synthetic Aperture Radar (InSAR) techniques, were used in this research to identify and evaluate this high mountain upper-slope potential hazard in Aniangzhai landslide. Considering the huge height difference and the steep slope of Aniangzhai landslide, an iterative route planning method was proposed and adopted to obtain a 3D model with 0.02 m resolution and a DEM with 0.25 m resolution by using UAV and LiDAR close-in flight method, respectively. Meter-level huge cracks were clearly identified by the high-resolution UAV 3D model and LiDAR data, which confirm that the location of these cracks is related to the morphological structure of this ancient landslide. Time series InSAR analysis reveals the activity of this high-altitude area, with a maximum LOS displacement rate of 15 cm/a. The combination of the above remote sensing technologies confirms and reveals the high potential risk and the reactivated condition of the upper-slope of Aniangzhai landslide. Through this found we show that the evolution of Aninangzhai landslide happened through four stages with a cascading effect. This paper proves the usefulness of an integrated method to successfully identify and evaluate the high-altitude upper-slope potential hazard, and compares the technical features of them, providing a reference for future works that aimed to mitigate the potential damage of the upper slope.

Keywords: Upper-slope potential landslides; LiDAR; InSAR; UAV; Cascading effect

Introduction

Landslides are commonly developed on steep upper-slopes in mountainous regions. These landslides are extremely difficult to be detected during their early stage of development. Once a landslide is destabilized, it could cause severe harm. Some good examples are the Xinmo Village landslide in Mao County in 2016 (Fan et al. 2017), the Yarlung Zangbo River landslide in Milin County, Tibet in 2018 (Jia et al. 2019), the Baige landslide in 2019 (Fan et al. 2019) and so on. This kind of landslides are generally located in mountainous areas with high altitude and large height differences, featuring steep terrain and complex topography.

Traditional manual methods to investigate this kind of landslides are typically limited by low efficiency, high cost, high risk and low accessibility. Remote sensing technology, characterized by its non-contact long-distance detection, can effectively overcome various limitations of traditional manual investigation, especially the difficulty in investigating potential hazards in high-mountain upper-slope, and the efficiency of work, which is significantly improved (Scaioni et al. 2014; Zhao and Lu 2018). UAV photogrammetry is economical, flexible, and enables the capture of high-resolution images for landslide investigation. Nowadays, UAV photogrammetry techniques have been extensively used in landslide analysis (Niethammer et al. 2012; Lucieer et al. 2014; Turner et al. 2015; Fernández et al. 2016; Yu et al. 2017; Fan et al. 2017, 2019; Eker et al. 2018; Rossi et al. 2018; Ma et al. 2019; Giordan et al. 2020; Sestras et al. 2021; Cheng et al. 2021). However, the surface covered by vegetation is difficult to be observed by UAV photogrammetry. LiDAR, which has the ability to penetrate vegetation and quickly acquire real high-resolution DEM data to some extent, is also being gradually applied in landslide identification and monitoring (Glenn et al. 2006; Eeckhaut et al. 2007; Burns et al. 2010; Ventura et al. 2011; Jaboyedoff et al. 2012; Wang et al. 2013; Tarolli 2014; Chu et al. 2014; Ortuño et al. 2017; Tomás et al. 2018; Görüm 2019; Xu et al. 2021). Nevertheless, the main drawback of UAV and LiDAR is that they are not able to detect tiny displacements (i.e. millimeter level), even though the displacements are very small during the initial stage of a landslide. In contrast, InSAR time series analysis enables to detect very small displacements (Zhou et al. 2009; Ferretti et al., 2007). This remote sensing technique has been widely used for early landslide identification and monitoring in recent years (Gabriel et al. 1989; Peyret et al. 2008; Wasowski and Bovenga 2014; Dai et al. 2016, 2020; Intrieri et al. 2018; Dong et al. 2018; Tomás et al. 2019; Zhang et al. 2021). Consequently, a single observation technology does not enable

the identification and evaluation of steep potential landslides comprehensively and accurately because of the existing limitations and complexity in mountainous regions. Therefore, a combination of multiple remote sensing technologies is needed.

On June 17, 2020, a sudden rainstorm fell in the Meilonggou area of Banshanmen Town, Danba County, Sichuan Province, resulted in a debris flow in Meilonggou that caused the blockage of the Xiaojinchuan River and formed a barrier lake. Subsequently, the post-failure flood caused a cascading effect, destabilizing the front edge of the foot of the ancient Aniangzhai landslide encompassing an area of about 0.62 km^2 (Zhao et al. 2021). A combination of in-situ investigation, remote sensing analyses, and simulations were performed to understand the failure mechanism (Zhu et al. 2021). Post-hazard surveys, remote sensing, and seismic signals were obtained to comprehensively analyze the evolution process of the landslide dam failure hazard chain (Yan et al. 2021). UAV and Terrestrial Laser Scanner (TLS) were used to obtain displacements of the failure caused by the June 17, 2020 event (Jiang et al. 2021) and InSAR was used to reveal the displacements of the slope before the June 17, 2020 event (Xia et al. 2021; Kuang et al. 2022). However, few works have been devoted to investigate the upper-slope of Aniangzhai landslide after the June 17, 2020 event, and the precise boundary of whole landslide is also not clear.

This paper combines three remote sensing technologies, including UAV photogrammetry, LiDAR and InSAR, to identify and evaluate the upper-slope of Aniangzhai landslide. A high potential risk on the upper-slope was revealed by multi-source remote sensing. The technical keys of acquiring high-resolution data of UAV and LiDAR in high mountain valleys are also discussed in this paper.

Study area

Aniangzhai landslide (102°01'44.8"E, 30°58'22.8″N) is located 20 km northeast of Danba County, Sichuan Province, China, which is 190 km straight line distance and 309 km driving distance from the provincial capital Chengdu. The study area is the transition zone of the first and second steps in China, with a typical alpine valley landscape and Tibetan plateau type monsoon climate. China's land terrain can be divided into three steps from west to east. The first step includes the Qinghai-Tibet Plateau and the Qaidam Basin with an average altitude of more than 4,000 m a.s.l.. The area of China's second step ladder accounts for about one-third of China's land area, with an average altitude of 1000-2000 m a.s.l.. The third step is mainly composed of plains and hills, with an average altitude below 500 m a.s.l.. The

annual average temperature is 14.2 ℃ in this area. Aniangzhai landslide is located at the confluence of the Xiaojinchuan River and Meilonggou ditch (**¡Error! No se encuentra el origen de la referencia.a**). G350 Road (also known as China Panda Avenue), which is the most important link between Danba County and Xiaojin County, runs along the banks of the Xiaojin River. There are hundreds of people living in Aniangzhai Village which is near the Aniangzhai landslide. The distance from the front edge to the tailing edge in the slope is 1.75 km and the difference in height is over 1000 m.

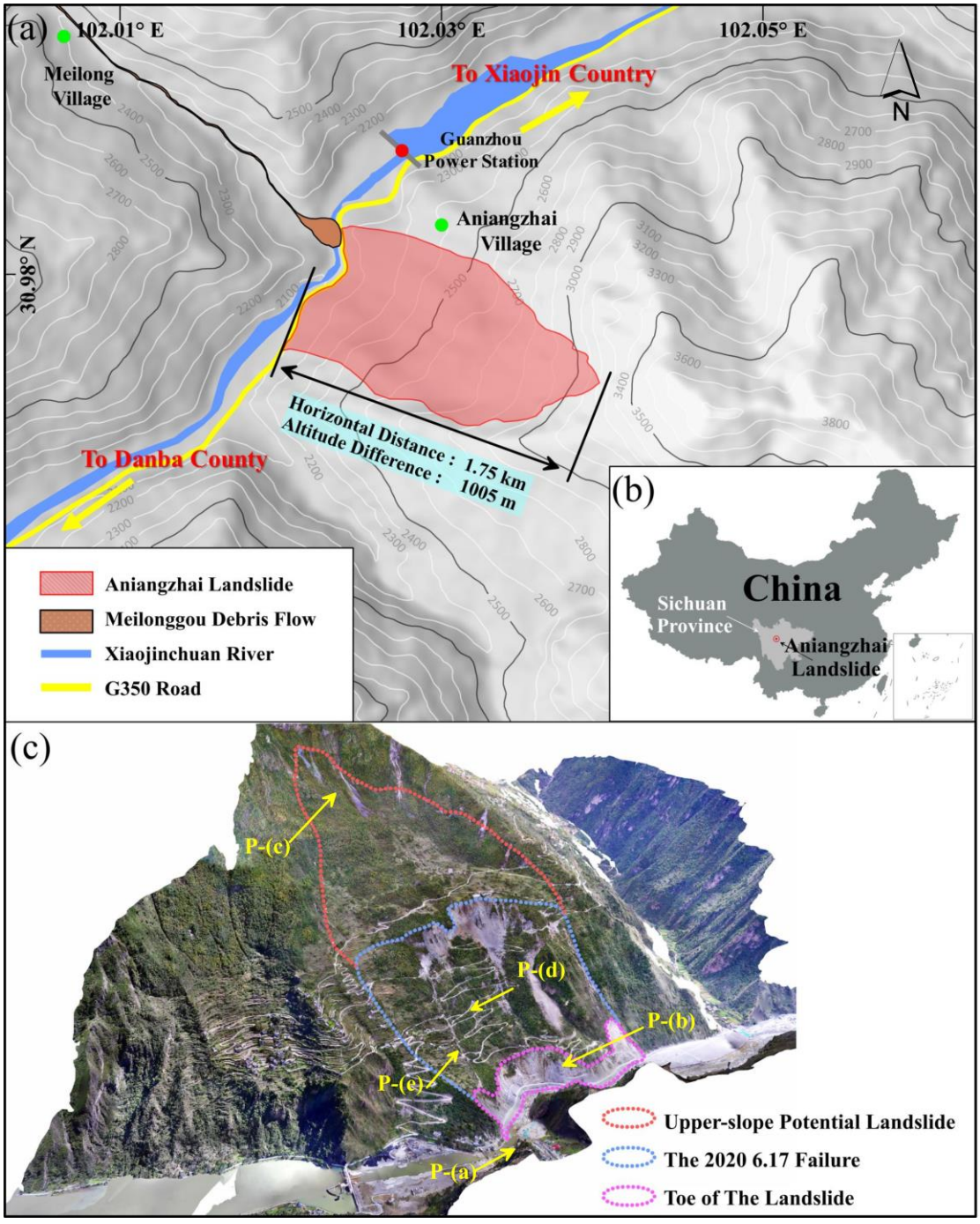

Fig. 1 Overview of the study area. (a) Topography maps of the study area. (b) Location of the study

area. (c) 3D model of the study area obtained by UAV. P-(a) to P(e) indicate the approximate location of the photos shown in Figure 2.

¡Error! No se encuentra el origen de la referencia.c illustrates a UAV 3D model acquired on 16 October 2021, in which three areas are highlighted with dashed lines. The area with magenta circle is the toe of the Aniangzhai landslide, which collapsed in the June 17, 2020 event (Zhao et al. 2021; Zhu et al. 2021; Yan et al. 2021), and the on-site photos are shown in **Fig.2a** and **Fig.2b** . The blue line region corresponds to the deduced failure of Aniangzhai ancient landslide after the collapse of the toe (Song et al. 2021; Zhu et al. 2021; Yan et al. 2021; Xia et al. 2021). Additionally, the upper-slope is highlighted by red circle in **¡Error! No se encuentra el origen de la referencia.c** and the on-site photo is shown in **Fig.2c**. Jiang et al. (2021) mentioned this area when they studied this landslide using UAV and TSL, but did not explored it in detail and did not determine the exact boundaries of the landslide. However, it can be seen that there are obvious cracks in the tailing edge of the area in the 3D model. Consequently, three remote methods have been used in this work to reveal the evolution of the upper-slope potential danger.

Fig.2 Field work photos of Aniangzhai landslide. (a) and (b) show the toe of the slope collapse related to Meilonggou debris flow. (c) Upper-slope area of Aniangzhai landslide. (d) (e) Tension cracks. The approximate locations of the pictures are shown in Figure 1.

Methods and data

A close flight method was adopted to obtain the high-resolution UAV 3D model and LiDAR data in this paper. Meanwhile, SBAS-InSAR technology was used to detect time series displacements information. These three remote sensing techniques are combined to carry out the research of the upper-slope potential

hazard of Aniangzhai landslide. The adopted workflow is depicted in **Fig. 3** and the data used in this study is shown in **Tab.1** and **Fig. 3c**.

Tab.1 Summary of the study data

Data	Resolution	Date	Equipment
UAV 3D model	0.02 m	2021.10.16	Share 102S
LiDAR data	0.25 m	2021.10.16	DJI L1
SAR images	2.33 m / 13.96 m	2020.06.20 – 2021.11.18	Sentinel-1A (ESA)

Acquisition and processing of UAV data

A DJI-M300 UAV equipped with a Share-102S five-lens oblique camera was used in this study. The DJI-M300 UAV had an integrated RTK positioning system that provided centimeter-level accuracy position POS (position and orientation system) information.

When using UAV for aerial photography, flight route needs to be laid out according to certain constraints. Relative flight height is a key parameter in UAV photogrammetry, which is directly related to the Ground Sample Distance (GSD) of the image. Therefore, the relative flight height setting was determined by the parameters of the aerial camera and GSD using next equation:

$$H = \frac{f \times GSD}{a} \quad (1)$$

Where H is the relative flight height in m; f is the focal length of the camera lens in mm; GSD is the ground sample distance in m; and a is the pixel size of camera in mm.

Therefore, it is important to maintain consistent relative flight height for images with consistent GSD. The study area belongs to an alpine canyon landscape with a height difference nearly 1000 meters. If the aerial photography operation is carried out according to the conventional 2D flight route, the same or similar relative aerial height cannot be guaranteed, which leads to an inconsistent GSD of the acquired images impeding the requirements of high resolution and high precision. In response to this problem, the method of laying a 3D coverage route based on existing DEM was proposed. Since the debris flow and the landslide disasters in the study area, and the high transmission towers built in recent years had changed the terrain, we could not directly lay out the 3D coverage route based on the SRTM-DEM. Consequently, an iterative DSM method to lay out a 3D flight route to cope with the aerial photography operation with huge height difference shown as **Fig. 3a** was adopted. Firstly, the common 2D route was

laid out based on SRTM-DEM, and the relative height was set larger to ensure flight safety and flight efficiency (the relative height of the 2D route in this study is between 400 and 1300 m). The position information and images were pre-processed and the aerial triangulation processed to quickly obtain a rough DSM with GSD of 5 m. Compared with SRTM-DEM, the rough DSM was more accurate and provided information of ground buildings, transmission towers, etc. Then, based on this rough DSM, we laid out a 3D route to keep consistent the relative flight height and keep away from obstacles such as transmission towers.

The designed GSD was 0.02 m and the relative flight height was calculated to be about 180 m in this study. Furthermore, the heading and side direction were overlapped over 75%. Finally, we got the 3D model with a GSD of 0.02 m.

Acquisition and processing of LiDAR data

A DJI-L1 LiDAR system was mounted on the DJI-M300 UAV for the capture of the point cloud. The relative flight height is also very important for Airborne-LiDAR operations, because the quality of the final acquired point cloud data is directly related to it. Like for the UAV photogrammetry, we also used the DSM-based 3D flight route for LiDAR surveying as shown in **Fig. 3a**. However, when carrying LiDAR for close ground flight to collect data, the laser beam center scattering characteristics must be taken into consideration. In order to ensure consistent point cloud density, it was needed to fly perpendicular to the contour. After obtaining the point cloud data, it was also necessary to classify the point cloud data and to extract the ground points to obtain a high precision and high-resolution DEM. The Progressive TIN Densification (PTD) was used to automatically extract the ground points (Axelsson 2000; Meng et al. 2010; Lin and Zhang 2014; Chen et al. 2021). The Triangulated Irregular Network (TIN) model was constructed based on these discrete ground points, and finally the elevation value was interpolated to generate a DEM with a resolution of 0.25 m. The DEM generated based on LiDAR data had a high resolution and a high precision, providing information about the real surface conditions under vegetation to some extent (Glenn et al. 2006; Eeckhaut et al. 2007). In this paper, we used Sky View Factory (SVF) (Guo et al. 2021) for DEM visualization, which enables to partially correct the limitations of poor local texture caused by a single light source in traditional mountain shade maps, and can provide a more comprehensive visual reflection of surface features, which is favorable for the analysis of landslides.

Processing of SBAS-InSAR

The small baseline differential SAR interferograms (SBAS-InSAR) technique (Berardino et al. 2002) is a method which enables to obtain time series of displacements and effectively overcomes the limitations of the traditional D-InSAR technique by time decoherence, spatial decoherence or atmospheric delay. SBAS-InSAR was used for this study because it works better in low coherence areas such as the mountainous areas of Southwest China (Zhang et al. 2018). The workflow of SBAS-InSAR is as follows: firstly, multi-scene images of different time periods in the same area were selected for precise coregistration, their time-space baselines were calculated, and multiple sets of interferometric pairs were combined by selecting suitable time-space baseline thresholds. Then differential interference, filtering and phase unwrapping were performed on these interferometric pairs. Finally, the displacements parameters of the freely formed short baseline sets of these interferometric pairs were estimated by using the least squares method or singular value decomposition method to obtain the time series displacements and surface displacement rates of the study area. The workflow is shown in **Fig. 3b**.

In this study, Sentinel-A C-band SAR images were used. In consideration of the geometric distortions in mountainous areas due to the side-looking geometry of InSAR (Dai et al. 2022), 42 descending images after June 17, 2020 event were used to analyze the evolution characteristics of the upper-slope after the disaster. The SRTM-DEM was used to assist images registration and remove topographic phase. Due to the poor coherence of Sentinel-1 data in this study area, we only selected interference pairs with a time baseline of less than 36 days.

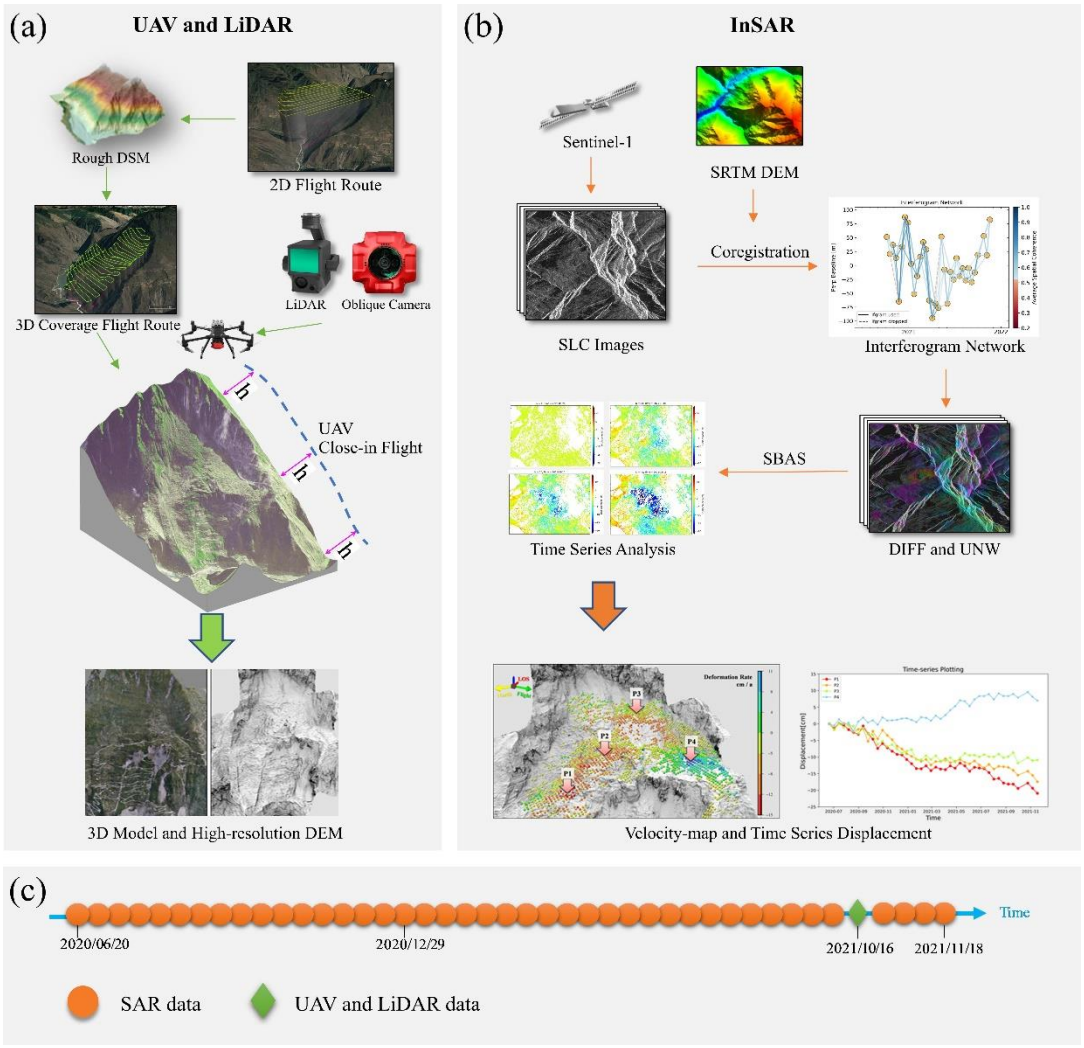

Fig. 3 Workflow adopted in this study. (a) UAV and LiDAR (b) InSAR. (c) Timeline of data acquisition. DSM: Digital Surface Model; SBAS: Small Baseline technique; DIFF: interferograms; UNW: Unwrapped interferograms.

Results

Analysis of UAV data

As the GSD of the UAV 3D model can reach the resolution of 2 cm, landslide features such as tensile cracks and shear cracks can be clearly identified on the 3D model to determine the landslide potential hazard boundary. According to the distribution of cracks (**Fig.4b-g**) and topographic elevation, the whole Aniangzhai landslide can be divided into 3 tiers and 7 areas as shown in **Fig.4a**.

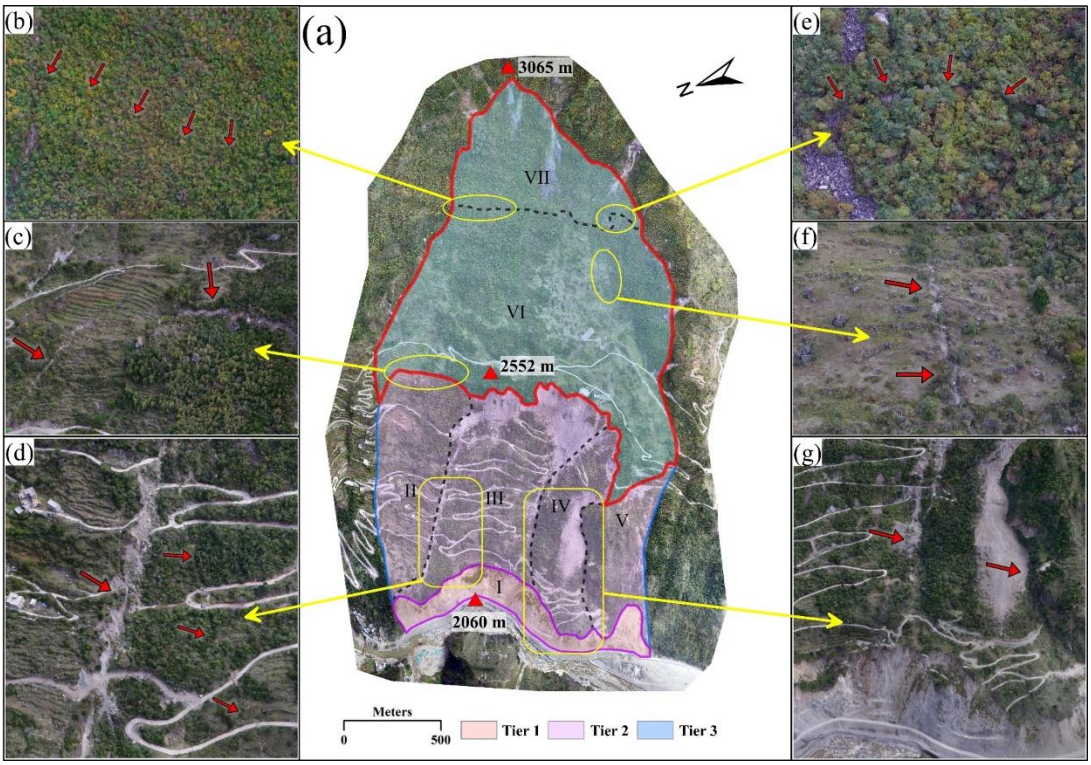

Fig.4 Zonation of Aniangzhai lanslide slope based on the 3D model. (a) Zonation of whole slope. (b) (c) (d) (e) (f) (g) Examples of cracks. Red arrows deliniate the location of the cracks.

Area I, located at the first tier, is the most front edge of the entire landslide body, with elevations ranging from 2060 to 2162 m a.s.l.. This area was the first to collapse due to the cascading effect caused by the impact of the debris flow. Due to the collapse, the anti-slip resistance was considerably reduced, inducing the failure of the second tier.

Areas II, III, IV, V belong to the second tier of the landslide, ranging from 2162 to 2556 m a.s.l.. Among them, the displacement in area III is the largest. Tension cracks at the tailing edge of this area are very obvious in the 3D model, and the scarp is also clearly visible. In addition, obvious tension shear cracks appeared at the juncture of these areas also at the landslide flanks both on the left and right sides.

Area VI and area VII are in the third tier with a difference in elevation over 500 m a.s.l.. The upper-slope is divided into two areas by an inconspicuous fissure (**Fig.4b and e**). Those potential hazards were not noticed by researchers because there were no obvious features on the tailing edge at the initial stage and it was difficult for personnel to reach this zone during the development of the field investigation. However, through the high-resolution 3D model collected on October 16, 2021 (**Fig. 5**¡Error! No se encuentra el origen de la referencia.), it can be seen that a complete arc-shaped crack appears on the crown of the landslide in this area, among which the width of the fissure at the rearmost edge position

D3 can reach 28.52 m, and the width of the fissure at other positions varied from 2 to 10 m. Thus, it can be tentatively judged that the landslide in the area VI and the area VII have also been activated and are currently in a creeping or sliding stage. As for the evolution process of this upper-slope, it needs to be analyzed combined with other information.

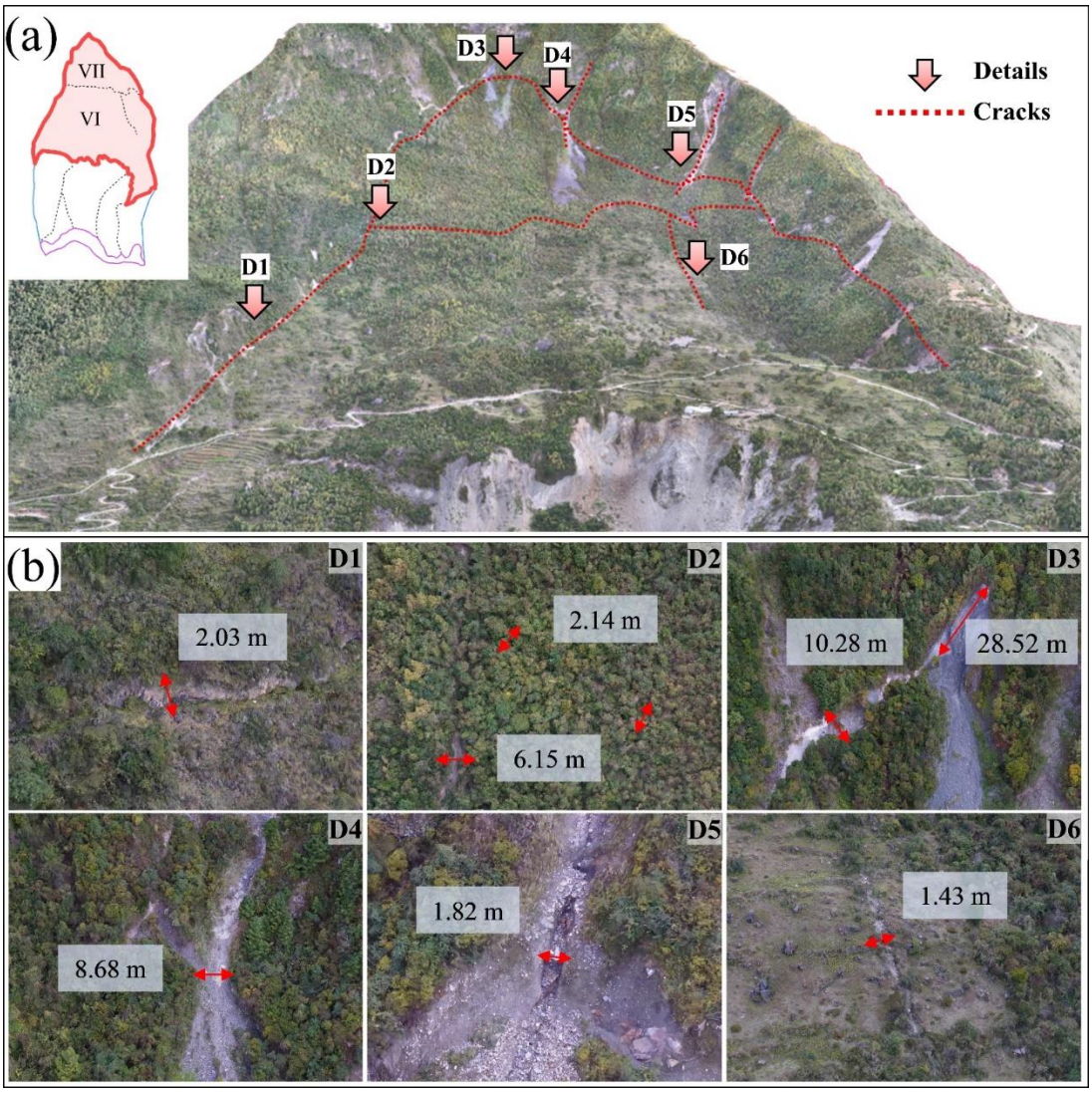

Fig. 5 Evaluation of the upper-slope (areas VI and VII) based on the obtained 3D model. (a) Overview of the distribution of cracks on the upper-slope. (b) Details of cracks.

Analysis of LiDAR data

Vegetation covers more than 85% of Aniangzhai landslide. For investigating the real surface morphology under its vegetation cover, the 0.25 m resolution DEM acquired by LiDAR is visualized by the SVF method shown in **Fig.6.** The ancient landslide accumulation body after removing vegetation is clearly visible and the scarps of the ancient landslide can also be recognized from the SVF map and slope maps as shown in Fig. 6a and Fig. 6b. From the details in Fig. 6c and Fig. 6d, it can be found that in the upper-

slope there is a clear visible trace between the sliding area and the stable area. Based on the above characteristics, we determined the boundaries of the landslide, and the arc-shaped fissure identified on the 3D model (Fig.5a) correspond with the ancient landslide boundary. Combined with the DEM-derived slope gradient map (Fig.6b), we can see that the rear part of the upper-slope is steep with an average slope higher than 30°, and the front part is gentle. This , it is a typical feature of ancient accumulation landslides accumulation. When the platform located below it (Area II – V) is destabilized, it is highly likely that the upper part of the ancient landslide is reactivated under the effect of gravity.” When the platform located below it (Area II – V) is destabilized, it is highly likely that the upper part of the ancient landslide is reactivated under the effect of gravity.

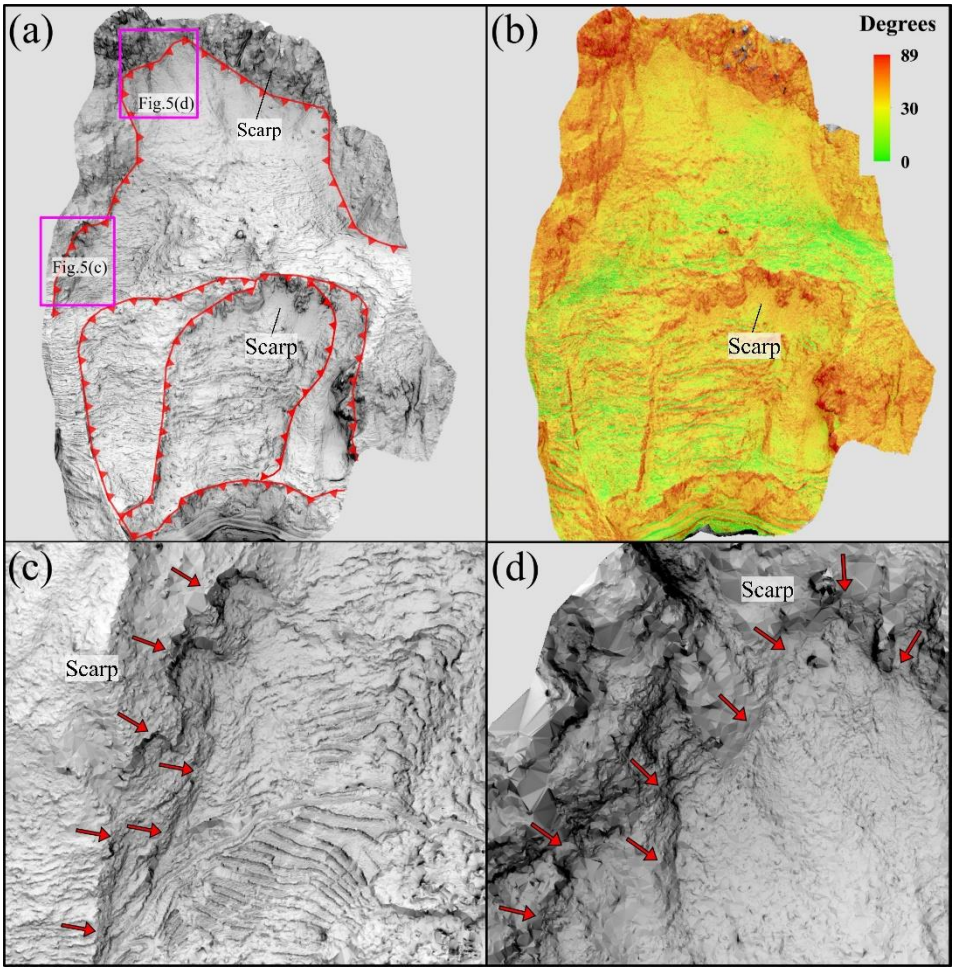

Fig.6 Analysis of the upper-slope based on LiDAR data. (a) SVF map. (b) Slope map. (c) (d) Details of the upper-slope. Red lines and the red arrows delineate the scarps.

Analysis of InSAR data

In order to further reveal the kinematic evolution process of the upper-slope potential landslide, the time series SBAS-InSAR technique was used. LOS displacement rates were obtained as shown in **Fig.7a**.

Negative red values indicate that the objects are far away from the satellite along the LOS direction and can be considered as a component of subsidence; Positive blue values indicate that the point is moving towards the satellite along the LOS direction and can be considered as a component of uplifting. The LOS displacement rate of the upper-slope varies from -15 to 11 cm/a. From **Fig.7a**, it can be found that the area near points P1, P2 and P3 shows downward displacements, while the area near point P4 shows uplift.

For further quantitative analysis, the time series displacements of points P1, P2, P3 and P4 are plotted, as shown in **Fig.7b**. The cumulative displacement of P1 is the largest, with a value of -20 cm from June 20, 2020 to November 18, 2021, revealing that this area is active since the occurrence of the June 17, 2020 event. By the end of January 2021, there was a deceleration and the slope gradually entered into a stable state. However, this stable state was only maintained until July 2021, when the slide reactivated again. The cumulative displacement of P2 is around -17 cm, and its time-series displacement curve was like P1. The cumulative displacement of P3 is around -11 cm, exhibiting activity from the beginning of the observation to the end of December 2020, and then becoming stable. Finally, the cumulative displacement of P4 is 11 cm. From the slope gradient shown in **Fig.6b**, it can be found that the area near the point P4 is a gentler platform with a certain anti-slip resistance that probably corresponds to the area of accumulation in which the soil is squeezed and bulged due to the sliding of the upper landsliding mass. It is worth noting that all the time series curves of P1-P3 show an obvious acceleration after September 2020, which coincides with the time point of activation of this region mentioned in the study published by Jiang et al. (2021).

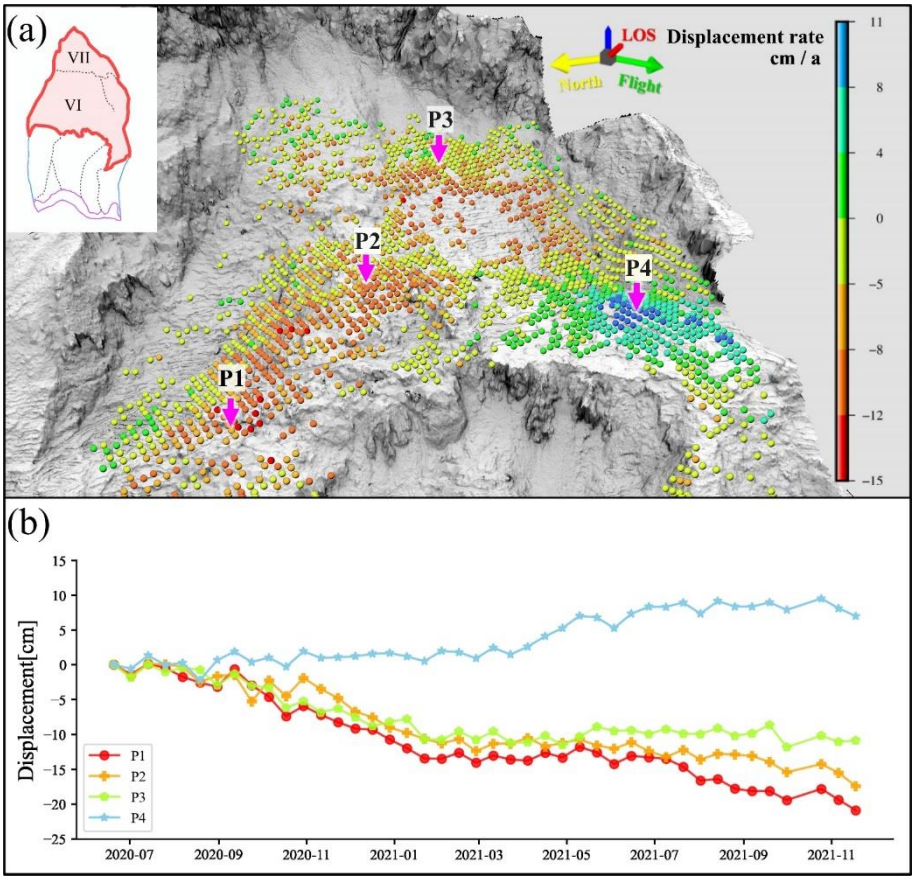

Fig.7 Kinematics of the upper-slope based on InSAR data. (a) Velocity map derived from SBAS-InSAR (b) Displacement time series plotting of some representative points.

Discussion

Evolution of Aniangzhai landslide

So far, the evolution of this event can be roughly divided into 4 stages shown in **Fig. 8**. It should be notes that this case study shows a clear example of cascading effect (Pescaroli and Alexander 2015) in which the impact of a physical event (i.e. rainfall) generated a sequence of events. First, the rainfall event occurred on June 17, 2020 in the Meilonggou area of Banshanmen Town, resulted in a mudslide that caused the blockage of the Xiaojinchuan River, formed a barrier lake and impacted the toe of the slope (stage 1 show in **Fig. 8a**). Then, during stage 2 (**Fig. 8b**), the toe of the ancient landslide collapsed in a short period. Due to the collapse of the toe, the tier-2 lost its support and was activated by gravity (stage 3 shown in **Fig. 8c**). Stages 1-3 have been described in detail by different scholars (Zhao et al. 2021, Zhu et al. 2021, Xia et al. 2021, Yan et al. 2021). Significant slippage occurred within 2-3 months after the activation of the tier-2. At the same time the toe of the tier-3 collapsed, reactivating the upper-slope landslide (Jiang et al. 2021), and then, the Aniangzhai landslide entered into stage 4 (**Fig. 8d**), which means that the entire ancient landslide became activated. By the

end of 2021, significant tension cracks appeared on the crown of upper-slope (**Fig. 5**) and InSAR data also detected displacement features in this area (**Fig.7**).

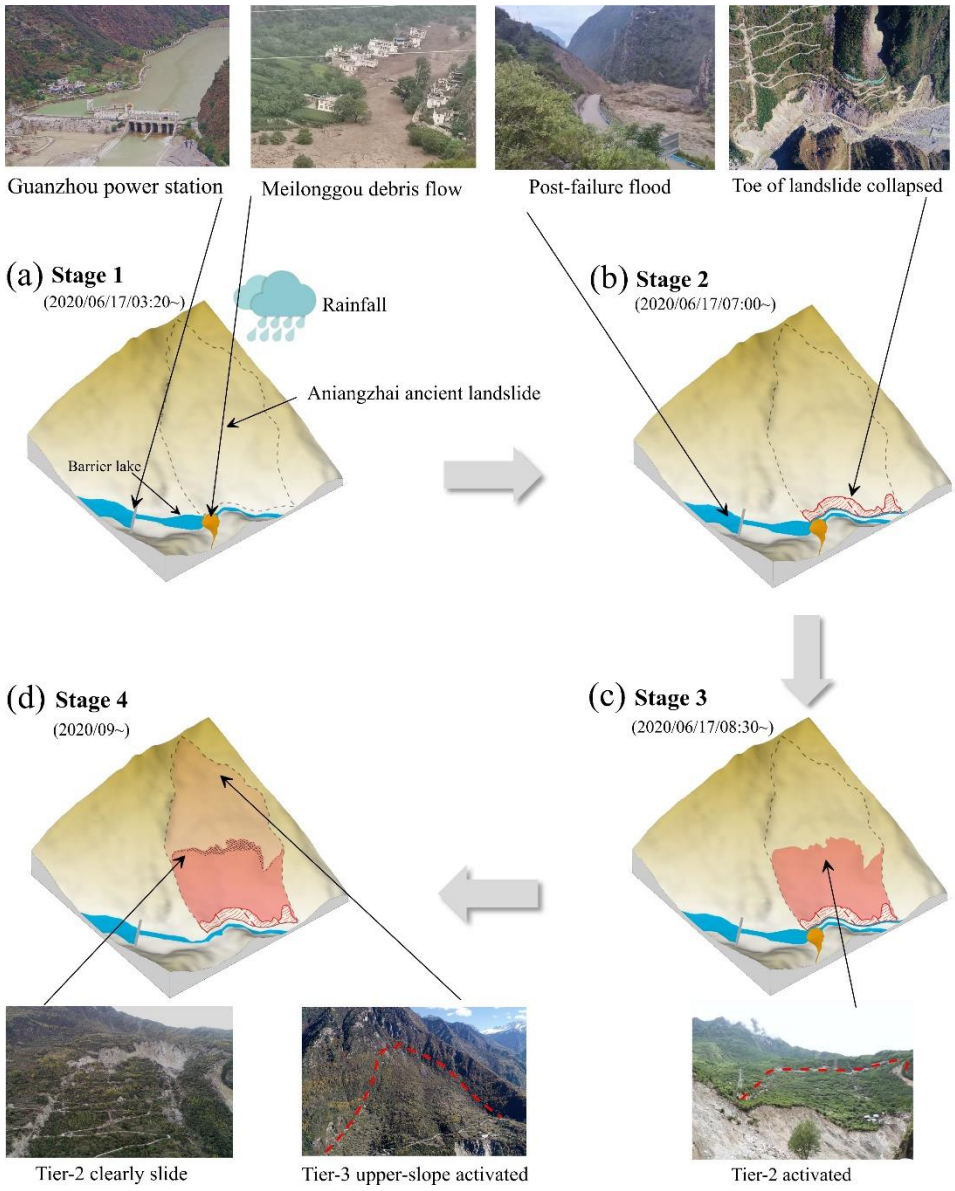

Fig. 8 Evolution of Aniangzhai landslide after the June 17, 2020 event.

Applicability analysis of multi-source remote sensing in landslides

The applicability, advantages and disadvantages of the three techniques in landslide analysis applications are summarized in this study, as shown in **Tab. 2**.

Tab. 2 Comparison of three remote sensing methods.

Methods	Products	Advantages	Disadvantages
UAV photogrammetry	High-resolution 3D-model Cracks and scarps	High-resolution and texture features,	Disturbed by vegetation

	identification	Customized acquisition	
LiDAR	High-resolution DEM Slope morphology analysis	Partial vegetation removal, Customized acquisition	Lack of textural features
InSAR	Time series displacements	Historic data, wide coverage and high-precision displacement information	Affected by vegetation, and geometrical distortions Non-customized acquisition

The high-resolution 3D model and images obtained by UAV photogrammetry have extremely obvious texture features. The GSD of the 3D model obtained by the 3D route-based UAV photogrammetry is as high as 2 cm. These data are very useful for the identification of landslide cracks, especially those with very small widths just developed in the early stage shown in **Fig. 5**. In the 3D model, it is possible to observe the upper-slope potential hazards that are inaccessible to personnel in a safe manner. Based on these signs and the cracks identified by the UAV data, the landslide can be zoned to facilitate subsequent research and management work. However, in areas with dense vegetation, UAV photogrammetry cannot observe the surface hidden below the vegetation. It should be noted that in southwest China landslides are often characterized by vegetation cover, which means an important limitation for the use of UAV photogrammetry. In contrast, LiDAR presents an inherent advantage in measuring vegetation-covered areas since it can partially penetrate vegetation to obtain surface information. Then, the point cloud data collected by LiDAR can be classified to remove vegetation and obtain high-resolution and high-precision DEM. Geomorphic features left by landslide movements such as circle chair-like landforms, steep canyons, and cracks are used to identify and delineate the extent of the landslides, especially for ancient landslides. Combined with the DEM-derived slope angle and slope direction information, the slope morphology can be analyzed. In this study, the determination of the exact boundary of the ancient landslide was almost entirely based on LiDAR data. However, point cloud data lacks texture information, and needs to be combined with UAV photogrammetry for landslides analysis, although LiDAR can only reach the centimeter level.

Finally, InSAR can detect tiny displacements and monitor millimeter-level displacements in those

areas exhibiting good coherence. The 12 days revisit period of the Sentinel-1 satellite provides the conditions for time series displacements analysis. Therefore, the evolution of the landslides can be analyzed based on it. In addition, for sudden events, the displacements characteristics can be traced back to the time before the event because of the existence of a long archive of satellite data. However InSAR has poor coherence in vegetation-covered areas with spatial and temporal decoherence. Furthermore, InSAR results are also affected by factors such as atmospheric delay.

Consequently, the combination of these three remote sensing technologies, namely UAV, LiDAR and InSAR, each of them with their own advantages and disadvantages (Xu et al., 2022), can effectively and accurately allow the identification of landslides, and is an indispensable way to study the evolutionary processes of potential landslides in a safer manner, especially in very steep and inaccessible mountain slopes.

Conclusions

In this paper, three kinds of remote sensing techniques, UAV, LiDAR and InSAR, were combined to evaluate the boundary extent, morphological structure and displacements characteristics of the Aniangzhai landslide.

The results of the study showed that the tension and shear cracks developed at the boundary of areas VI and VII were discovered from the analysis of the UAV 3D model. This model also allowed to divide the landslide into three tiers and seven areas. The accumulation features hidden under vegetation caused by the ancient landslide in upper-slope were identified using the LiDAR-derived DEM, and the accumulation boundary was basically consistent with the location of the cracks discovered by the UAV 3D model. Time series displacements information of the upper-slope extracted by SBAS-InSAR revealed that this region was active, exhibiting maximum displacements up to 15 cm/a in the LOS direction. Based on the above information, it can be determined that tier-3 represents a potential hazard, since the entire landslide is fully active and needs further monitoring.

This work illustrates how the combined use of the three remote sensing methods mentioned above can effectively contribute to identify and evaluate the potential hazard of landslides. The main conclusion drawn is that multi-source remote sensing enables the exploitation of the complementarities of different techniques, providing new references and views to state the potential risk of landslides on high and steep

landslides in complex mountainous region.

Acknowledgements

This research was funded by the National Key Research and Development Program of China (grant number 2021YFB3901403), the National Natural Science Foundation of China Major Program (41941019), the National Natural Science Foundation of China (41801391), the State Key Laboratory of Geohazard Prevention and Geoenvironment Protection Independent Research Project (SKLGP2020Z012), the fellowship of China Postdoctoral Science Foundation (2020M673322), the ESA-MOST China DRAGON-5 project (ref. 59339) and a project on the identification and monitoring of potential geological hazards with remote sensing in Sichuan Province (510201202076888).

Conflict of Interests

The authors declare no competing interests.

Reference

Axelsson P (2000) DEM generation from laser scanner data using adaptive TIN models. International archives of photogrammetry and remote sensing 33:110–117

Berardino P, Fornaro G, Lanari R, Sansosti E (2002) A new algorithm for surface deformation monitoring based on small baseline differential SAR interferograms. IEEE Transactions on Geoscience and Remote Sensing 40:2375–2383. https://doi.org/10.1109/TGRS.2002.803792

Burns WJ, Coe JA, Kaya BS, Ma L (2010) Analysis of Elevation Changes Detected from Multi-Temporal LiDAR Surveys in Forested Landslide Terrain in Western Oregon. Environmental and Engineering Geoscience 16:315–341. https://doi.org/10.2113/gseegeosci.16.4.315

Chen C, Guo J, Wu H, et al (2021) Performance Comparison of Filtering Algorithms for High-Density Airborne LiDAR Point Clouds over Complex LandScapes. Remote Sensing 13:2663. https://doi.org/10.3390/rs13142663

Cheng Z, Gong W, Tang H, et al (2021) UAV photogrammetry-based remote sensing and preliminary assessment of the behavior of a landslide in Guizhou, China. Engineering Geology 289:106172. https://doi.org/10.1016/j.enggeo.2021.106172

Chu H-J, Wang C-K, Huang M-L, et al (2014) Effect of point density and interpolation of LiDAR-

derived high-resolution DEMs on landscape scarp identification. GIScience & Remote Sensing 51:731–747. https://doi.org/10.1080/15481603.2014.980086

Dai K, Li Z, Tomás R, et al (2016) Monitoring activity at the Daguangbao mega-landslide (China) using Sentinel-1 TOPS time series interferometry. Remote Sensing of Environment 186:501–513. https://doi.org/10.1016/j.rse.2016.09.009

Dai K, Li Z, Xu Q, et al (2020) Entering the Era of Earth Observation-Based Landslide Warning Systems: A Novel and Exciting Framework. IEEE Geoscience and Remote Sensing Magazine 8:136–153. https://doi.org/10.1109/MGRS.2019.2954395

Dai K, Deng J, Xu Q, et al (2022). Interpretation and sensitivity analysis of the LOS displacements from InSAR in landslide measurement. GIScience & Remote Sensing

Dong J, Zhang L, Tang M, et al (2018) Mapping landslide surface displacements with time series SAR interferometry by combining persistent and distributed scatterers: A case study of Jiaju landslide in Danba, China. Remote Sensing of Environment 205:180–198. https://doi.org/10.1016/j.rse.2017.11.022

Eeckhaut MVD, Poesen J, Verstraeten G, et al (2007) Use of LIDAR-derived images for mapping old landslides under forest. Earth Surf Process Landforms 32:754–769. https://doi.org/10.1002/esp.1417

Eker R, Aydın A, Hübl J (2018) Unmanned aerial vehicle (UAV)-based monitoring of a landslide: Gallenzerkogel landslide (Ybbs-Lower Austria) case study. Environ Monit Assess 190:1–14. https://doi.org/10.1007/s10661-017-6402-8

Fan X, Xu Q, Alonso-Rodriguez A, et al (2019) Successive landsliding and damming of the Jinsha River in eastern Tibet, China: prime investigation, early warning, and emergency response. Landslides 16:1003–1020. https://doi.org/10.1007/s10346-019-01159-x

Fan X, Xu Q, Scaringi G, et al (2017) Failure mechanism and kinematics of the deadly June 24th 2017 Xinmo landslide, Maoxian, Sichuan, China. Landslides 14:2129–2146. https://doi.org/10.1007/s10346-017-0907-7

Ferretti, A., et al. (2007). "Submillimeter Accuracy of InSAR Time Series: Experimental Validation." IEEE Transactions on Geoscience and Remote Sensing 45(5): 1142-1153.

Fernández T, Pérez JL, Cardenal J, et al (2016) Analysis of Landslide Evolution Affecting Olive Groves Using UAV and Photogrammetric Techniques. Remote Sensing 8:837. https://doi.org/10.3390/rs8100837

Gabriel AK, Goldstein RM, Zebker HA (1989) Mapping small elevation changes over large areas: Differential radar interferometry. Journal of Geophysical Research: Solid Earth 94:9183–9191

Giordan D, Adams MS, Aicardi I, et al (2020) The use of unmanned aerial vehicles (UAVs) for

engineering geology applications. Bull Eng Geol Environ 79:3437–3481. https://doi.org/10.1007/s10064-020-01766-2

Glenn NF, Streutker DR, Chadwick DJ, et al (2006) Analysis of LiDAR-derived topographic information for characterizing and differentiating landslide morphology and activity. Geomorphology 73:131–148. https://doi.org/10.1016/j.geomorph.2005.07.006

Görüm T (2019) Landslide recognition and mapping in a mixed forest environment from airborne LiDAR data. Engineering Geology 258:105155. https://doi.org/10.1016/j.enggeo.2019.105155

Guo C, Xu Q, Dong X, et al (2021) Landslide recognition based on SVF terrain visualization method: a case study of a typical landslide in Danba, Sichuan, China. Journal of Chengdu University of Technology (Science and Technology Edition) 48:705–713 (In Chinese)

Intrieri E, Raspini F, Fumagalli A, et al (2018) The Maoxian landslide as seen from space: detecting precursors of failure with Sentinel-1 data. Landslides 15:123–133. https://doi.org/10.1007/s10346-017-0915-7

Jaboyedoff M, Oppikofer T, Abellán A, et al (2012) Use of LIDAR in landslide investigations: a review. Nat Hazards 61:5–28. https://doi.org/10.1007/s11069-010-9634-2

Jia H, Chen F, Pan D (2019) Disaster Chain Analysis of Avalanche and Landslide and the River Blocking Dam of the Yarlung Zangbo River in Milin County of Tibet on 17 and 29 October 2018. International Journal of Environmental Research and Public Health 16:4707. https://doi.org/10.3390/ijerph16234707

Jiang N, Li H, Hu Y, et al (2021) A Monitoring Method Integrating Terrestrial Laser Scanning and Unmanned Aerial Vehicles for Different Landslide Deformation Patterns. IEEE J Sel Top Appl Earth Observations Remote Sensing 14:10242–10255. https://doi.org/10.1109/JSTARS.2021.3117946

Kuang J, Ng AH-M, Ge L (2022) Displacement characterization and spatial-temporal evolution of the 2020 aniangzhai landslide in danba county using time-series insar and multi-temporal optical dataset. Remote Sensing v 14, n 1:. https://doi.org/10.3390/rs14010068

Lin X, Zhang J (2014) Segmentation-based filtering of airborne LiDAR point clouds by progressive densification of terrain segments. Remote Sensing 6:1294–1326

Lucieer A, Jong SM de, Turner D (2014) Mapping landslide displacements using Structure from Motion (SfM) and image correlation of multi-temporal UAV photography. Progress in Physical Geography: Earth and Environment 38:97–116. https://doi.org/10.1177/0309133313515293

Ma S, Xu C, Shao X, et al (2019) Geometric and kinematic features of a landslide in Mabian Sichuan, China, derived from UAV photography. Landslides 16:373–381. https://doi.org/10.1007/s10346-018-1104-z

Meng X, Currit N, Zhao K (2010) Ground Filtering Algorithms for Airborne LiDAR Data: A Review of Critical Issues. Remote Sensing 2:833–860. https://doi.org/10.3390/rs2030833

Niethammer U, James MR, Rothmund S, et al (2012) UAV-based remote sensing of the Super-Sauze landslide: Evaluation and results. Engineering Geology 128:2–11. https://doi.org/10.1016/j.enggeo.2011.03.012

Ortuño M, Guinau M, Calvet J, et al (2017) Potential of airborne LiDAR data analysis to detect subtle landforms of slope failure: Portainé, Central Pyrenees. Geomorphology 295:364–382

Pescaroli G, Alexander D (2015) A definition of cascading disasters and cascading effects: Going beyond the "toppling dominos" metaphor. Planet@ risk 3:58–67

Peyret M, Djamour Y, Rizza M, et al (2008) Monitoring of the large slow Kahrod landslide in Alborz mountain range (Iran) by GPS and SAR interferometry. Engineering Geology 100:131–141

Rossi G, Tanteri L, Tofani V, et al (2018) Multitemporal UAV surveys for landslide mapping and characterization. Landslides 15:1045–1052. https://doi.org/10.1007/s10346-018-0978-0

Scaioni M, Longoni L, Melillo V, Papini M (2014) Remote Sensing for Landslide Investigations: An Overview of Recent Achievements and Perspectives. Remote Sensing 6:9600–9652. https://doi.org/10.3390/rs6109600

Sestras P, Bilașco Ștefan, Roșca S, et al (2021) Geodetic and UAV Monitoring in the Sustainable Management of Shallow Landslides and Erosion of a Susceptible Urban Environment. Remote Sensing 13:385. https://doi.org/10.3390/rs13030385

Song Y, Hu G, He N, et al. Preliminary analysis on the characteristics and causes of landslide in "6·17" Aniangzhai village in Danba County. Science Technology and Engineering 2021,21 (22):9243-9249. (In Chinese)

Tarolli P (2014) High-resolution topography for understanding Earth surface processes: Opportunities and challenges. Geomorphology 216:295–312. https://doi.org/10.1016/j.geomorph.2014.03.008

Tomás R, Abellán A, Cano M, et al (2018) A multidisciplinary approach for the investigation of a rock spreading on an urban slope. Landslides 15:199–217

Tomás R, Pagán JI, Navarro JA, et al (2019) Semi-automatic identification and pre-screening of geological–geotechnical deformational processes using persistent scatterer interferometry datasets. Remote Sensing 11:1675

Turner D, Lucieer A, de Jong S (2015) Time Series Analysis of Landslide Dynamics Using an Unmanned Aerial Vehicle (UAV). Remote Sensing 7:1736–1757. https://doi.org/10.3390/rs70201736

Ventura G, Vilardo G, Terranova C, Sessa EB (2011) Tracking and evolution of complex active landslides by multi-temporal airborne LiDAR data: The Montaguto landslide (Southern Italy). Remote Sensing of Environment 115:3237–3248. https://doi.org/10.1016/j.rse.2011.07.007

Wang G, Joyce J, Phillips D, et al (2013) Delineating and defining the boundaries of an active landslide in the rainforest of Puerto Rico using a combination of airborne and terrestrial LIDAR data. Landslides 10:503–513. https://doi.org/10.1007/s10346-013-0400-x

Wasowski J, Bovenga F (2014) Investigating landslides and unstable slopes with satellite Multi Temporal Interferometry: Current issues and future perspectives. Engineering Geology 174:103–138

Xia Z, Motagh M, Li T, Roessner S (2021) The June 2020 Aniangzhai landslide in Sichuan Province, Southwest China: slope instability analysis from radar and optical satellite remote sensing data. Landslides 1–17. https://doi.org/10.1007/s10346-021-01777-4

Xu Q, Guo C, Dong X, et al (2021) Mapping and Characterizing Displacements of Landslides with InSAR and Airborne LiDAR Technologies: A Case Study of Danba County, Southwest China. Remote Sensing 13:4234. https://doi.org/10.3390/rs13214234

Xu Q, Zhu X, Li W, et al (2022) Technical progress of space-air-ground collaborative monitoring of landslide. Acta Geodaetica et Cartographica Sinica. 51(7), 1416–1436 (in Chinese).

Yan Y, Cui Y, Liu D, et al (2021) Seismic signal characteristics and interpretation of the 2020 “6.17” Danba landslide dam failure hazard chain process. Landslides 18:2175–2192. https://doi.org/10.1007/s10346-021-01657-x

Yu M, Huang Y, Zhou J, Mao L (2017) Modeling of landslide topography based on micro-unmanned aerial vehicle photography and structure-from-motion. Environ Earth Sci 76:1–9. https://doi.org/10.1007/s12665-017-6860-x

Zhang L, Dai K, Deng J, et al (2021) Identifying Potential Landslides by Stacking-InSAR in Southwestern China and Its Performance Comparison with SBAS-InSAR. Remote Sensing 13:3662

Zhang L, Liao M, Dong J, Xu Q and Gong J (2018) Early detection of landslide hazards in mountainous areas of west China using time series interferometry—A case study of Danba, Sichuan. Journal of Chengdu University of Technology (Science and Technology Edition) (12),2039-2049. doi:10.13203/j.whugis20180181.

Zhao B, Zhang H, Liao H, et al (2021) Emergency response to the reactivated Aniangzhai landslide resulting from a rainstorm-triggered debris flow, Sichuan Province, China. Landslides 18:1115–1130

Zhao C, Lu Z (2018) Remote Sensing of Landslides—A Review. Remote Sensing 10:279. https://doi.org/10.3390/rs10020279

Zhou X, Chang N-B, Li S (2009) Applications of SAR Interferometry in Earth and Environmental Science Research. Sensors 9:1876–1912. https://doi.org/10.3390/s90301876

Zhu L, He S, Qin H, et al (2021) Analyzing the multi-hazard chain induced by a debris flow in Xiaojinchuan River, Sichuan, China. Engineering Geology 293:106280